Microscopic structure of molecularly thin confined liquid-crystal films

Thomas Gruhn* and Martin Schoen†
Institut für Theoretische Physik, Sekretariat PN 7-1, Technische Universität Berlin, Hardenbergstrasse 36, D-10623 Berlin, Germany
(Received 19 September 1996)

The microscopic structure of a molecularly thin liquid-crystal film confined between two plane parallel surfaces (i.e., walls) composed of rigidly fixed atoms is investigated in grand canonical ensemble Monte Carlo simulations in which the temperature T, the chemical potential μ, and the wall separation s_z are the relevant thermodynamic state variables. These conditions correspond to those encountered in related experiments employing the *surface forces apparatus* (SFA). Wall atoms are distributed according to the (100) configuration of a face-centered cubic (fcc) lattice. Film molecules interact with each other via the Gay-Berne potential which may be viewed as a Lennard-Jones (12,6) potential modified to account for the anisotropy of the interaction between two ellipsoidal film molecules. Parameters governing the film-wall interaction are chosen such that molecules tend to arrange their symmetry axes parallel with the plane of a wall (i.e., the x-y plane). The thermodynamic state of a bulk phase in equilibrium with the confined film pertains to the isotropic phase of the Gay-Berne fluid, so that preferred orientations in the film are unambiguously ascribed to confinement (i.e., to the presence of the walls). In general, film structure is characterized by stratification, that is, the tendency of film molecules to arrange their centers of mass in individual strata parallel with the walls. The strata are more diffuse than in films composed of ''simple'' molecules without rotational degrees of freedom due to a larger geometric incompatibility between film and wall structure and to orientability of film molecules in the present model. As s_z is increased at fixed T and μ, molecularly thin liquid-crystal films undergo complex structural changes resulting from a competition between wall-induced orientation and lack of space. These effects are analyzed in depth by density-alignment histograms and correlated with variations of the normal stress T_{zz} exerted by the film on the walls. The normal stress, which is in principle accessible in SFA experiments, depends strongly on s_z even in rather thick films, indicating the importance of cooperative wall-induced phenomena for materials properties of confined liquid-crystal films. [S1063-651X(97)04702-8]

PACS number(s): 61.30.Cz, 68.45.−v, 61.20.Ja, 82.65.Dp

I. INTRODUCTION

If condensed phases like, for instance, liquid crystals are confined to a volume V of some container, two different spatial regions are discernible provided V is macroscopic. At points $\{\boldsymbol{r}\}$ sufficiently far removed from any container wall the microscopic structure of the liquid crystal is solely dictated by the thermodynamic state. This so-defined bulk region may be anisotropic or isotropic depending on whether or not a preferred molecular orientation exists. Orientability of liquid-crystal molecules gives rise to nematic or smectic (bulk) mesophases in addition to an isotropic phase typical of ''simple'' bulk fluids without rotational degrees of freedom. If, on the other hand, one approaches a container wall sufficiently closely, the symmetry of the liquid crystal is dictated by the wall which represents a permanent solid interface or, from a more abstract perspective, may be viewed as an external field to which liquid-crystal molecules are exposed. In other words, in the immediate neighborhood of a wall a thin (vicinal) film exists whose microscopic structure is not completely determined by the thermodynamic state but also to some extent by the nature of the wall. For an isotropic bulk phase the thickness of a liquid-crystal film is related to the range of the potential characterizing the interaction between film molecules and the wall and is therefore microscopic in size, not exceeding a few molecular ''diameters.'' Then, the very different extent of bulk region and vicinal film permits one to safely ignore the impact of the latter on the former under the tacit proviso of a macroscopic V.

However, V does not have to be macroscopic under all circumstances. On the contrary, it can be quite tiny to the extent that the distance between the walls in one or more dimensions becomes comparable to the range of the fluid-wall potential so that a bulk phase in the above sense is absent. Intuitively one would then expect properties of a liquid-crystal vicinal film to differ markedly from those of a corresponding bulk liquid crystal under identical thermodynamic conditions. The physics of a microscopically thin confined liquid crystal is, however, not just an arcane academic playground but of technological importance. For instance, spatial and orientational structures of liquid-crystal films between solid interfaces are relevant for the development of new optimized displays [1]. In mechanical engineering, on the other hand, one is frequently confronted with friction between movable machine parts and wear. The impact of these ultimately destructive phenomena can be reduced by lubricants. In many cases it is commercially desirable to miniaturize certain machine parts so that the lubricant becomes a molecularly thin confined film [2]. In this regard liquid-crystal films are of great interest because they exhibit a much lower frictional resistance under high loads than conventional lubricants [3].

Because of advances in technology, properties of thin confined films are not only within experimental reach but can

*Electronic address: T.Gruhn@physik.tu-berlin.de
†Electronic address: M.Schoen@physik.tu-berlin.de

nowadays be measured almost routinely on a molecular scale. A particularly prominent experiment in this regard involves the so-called *surface forces apparatus* (SFA) by which rheological properties of confined molecularly thin films can be measured [4]. The films consist of rather different molecules, ranging from long-chain (e.g., hexadecane) or spheroidal [e.g., octamethylcyclotetrasiloxane (OMCTS)] hydrocarbons [5] to liquid crystals [e.g., 4-cyano-4′-octylbiphenyl (8CB)] [6]. In the SFA a thin film is confined between the surfaces of two cylinders which are arranged such that their axes are at right angles. The surfaces are traditionally covered with thin mica sheets which permit measurements of surface separation by optical techniques [4]. Cylinder radii are macroscopic so that the surfaces may be taken as parallel on a molecular length scale. In addition, they may be perceived as planar since mica can be prepared with atomic smoothness over molecularly large areas. This setup is immersed in a bulk reservoir of the same fluid of which the film consists. Thus at thermodynamic equilibrium temperature T and chemical potential μ are equal in both subsystems (i.e., film and bulk reservoir). By exerting an external stress in the direction normal to the surfaces, the film's thickness can be altered by either expelling molecules from it or by imbibing them from the reservoir until thermodynamic and mechanical equilibrium is reestablished, that is, until the stress exerted by the film on the surfaces equals the applied normal stress. If one displays this normal stress T_{zz} as a function of surface separation s_z, a damped oscillatory curve obtains in many cases (see, for instance, Fig. 1 in [5]). The oscillations, which are detected only if the molecular structure of film molecules matches the crystallographic structure of the surfaces to a minimum extent, are attributed to stratification, that is, the tendency of film molecules to arrange themselves in individual strata parallel with the surfaces. As a phenomenon occurring on a microscopic length scale, stratification to date cannot be observed directly in SFA experiments but has been established by computer simulations of SFA models involving films of ''simple'' fluids consisting of spherical particles (see [7], and references therein). A quantitative measure of stratification in these simulations is the local density which is a damped oscillatory function of position with respect to the walls. Its peaks, which in a ''simple''-fluid film at microscopically small s_z are quite narrow and tall, represent well-localized individual strata of film molecules. Stratification is caused by mere confinement, is unique in the sense that it is largely independent of the precise form of the film-wall interaction [8], and is accompanied by subtle order-disorder phase transitions as far as simple fluids are concerned [9,10]. If, on the other hand, complex fluids like liquid crystals are employed, aspects of a confined film's structure on a mesoscopic scale ranging from, say, nanometers to micrometers are now accessible experimentally by a modification of the *classic* SFA which combines the stress-measurement capability of the latter with x-ray diffraction [11]. In this so-called XSFA high-energy synchrotron radiation has recently been utilized to determine the orientation of a confined smectic liquid-crystalline film and its dependence on the ''softness'' of the confining surfaces [12].

From a theoretical perspective, several approaches are available to describe liquid-crystalline fluids in the presence of surfaces. A simple one, restricted to the nematic liquid-crystal phase, describes the preferred local molecular orientation by a director field. After spatial discretization the equilibrium director field can be obtained for any given boundary condition in the presence of external fields by solving a relaxation equation [13] or by minimizing the Frank free energy [14]. However, this approach disregards spatial variations of the density. A lattice model was also used by Dadmun and Muthukumar [15] to simulate a confined semiflexible liquid-crystal film. They report a strong dependence of the isotropic-nematic phase transition on the adsorption strength of the surface [15]. A more realistic microscopic picture of liquid crystals is achieved through models in which molecules are permitted to translate and rotate freely. Because of their complexity these models can only be studied in computer simulations. Examples include ellipsoidal [16,17], cylindrical [16], or needle-shaped particles [18] with either ''soft'' or ''hard'' interaction potentials. A realistic but still sufficiently simple description of the liquid-crystal intermolecular interaction is provided by the Gay-Berne model which is based on a Lennard-Jones potential modified for ellipsoidal particles [19]. For a certain set of potential parameters its bulk phase diagram is completely known and includes an isotropic and a nematic phase as well as some smectic-*B*-like phases [20]. In the nematic region the model was used to determine the temperature dependence of the elastic coefficients, including surface coefficients [21]. For a Gay-Berne film between plane parallel structureless (i.e., smooth) surfaces a wall-induced smectic-*A* structure was reported in [22,23] where temperature T and density n are chosen such that a corresponding bulk fluid is nematic. The fluid-wall interaction was chosen to be homeotropic.

Unfortunately, none of these investigations are directly applicable to XSFA experiments because the confined film is treated as a thermodynamically closed system with a fixed number of molecules whereas in the XSFA the film is open to the bulk reservoir, capable of exchanging matter with it. Exchange of matter between the confined film and the bulk reservoir, on the other hand, has important consequences for phase transitions particularly in cases of severe confinement (i.e., in very thin films) [24]. This observation and our interest in structure and materials properties of thin confined liquid-crystalline films under conditions encountered in the XSFA tempted us to employ the grand canonical ensemble Monte Carlo (GCEMC) method in this work. Since we wish to concentrate on the impact of confinement on the microscopic structure, we deliberately selected thermodynamic states for which a bulk liquid crystal is isotropic. Any preferred orientation of molecules in the confined film can then be attributed unambiguously to confinement effects. Results of our study are presented in Sec. IV. Section III is devoted to a derivation of molecular expressions for thermophysical properties of interest. We begin, however, in Sec. II with a description of our model system.

II. THE MODEL

We consider a film composed of N ellipsoidal molecules confined between two planar walls. Each wall is composed of an array of N_s spherically symmetric atoms distributed across the plane of the wall according to the (100) configu-

ration of the face-centered cubic (fcc) lattice. The walls are in registry, that is, they are aligned such that corresponding atoms in the two walls are always exactly opposite each other. Coordinates of a given atom (2) in the upper wall ($z=s_z$) are related to those of its counterpart (1) in the lower wall ($z=0$) by

$$\begin{aligned} x_2 &= x_1, \\ y_2 &= y_1, \\ z_2 &= z_1 + s_z = s_z. \end{aligned} \tag{1}$$

Assuming pairwise additivity of all interactions, the total configurational energy U can be written as

$$\begin{aligned} U &= U_{FF} + \sum_{k=1}^{2} U_{FW}^{(k)} \\ &= \frac{1}{2}\sum_{i=1}^{N}\sum_{j\neq i}^{N} u_{ff} + \sum_{k=1}^{2}\sum_{i=1}^{N}\left[\sum_{j=1}^{N_s} u_{fw}^{(k)} + u_{hw}(z_i)\right], \end{aligned} \tag{2}$$

where U_{FF} and $U_{FW}^{(k)}$ denote film-film and film-wall contributions, respectively; u_{ff} and $u_{fw}^{(k)}$ are the associated interaction potentials, and superscript k refers to lower ($k=1$) and upper ($k=2$) wall. A hard-wall background

$$u_{hw}(z_i) = \begin{cases} 0, & 0 < z_i < s_z \\ \infty, & z_i \leqslant 0,\ z_i \geqslant s_z \end{cases} \tag{3}$$

is formally imposed to define the distance between the walls rigorously despite their otherwise discrete (i.e., atomic) nature. However, wall atoms are so densely packed that during the course of a simulation film molecules never interact with the hard wall due to the finite range of the repulsive part of $u_{fw}^{(k)}$ [see Eq. (9) below].

We employ the Gay-Berne potential [19] for u_{ff} which provides a reasonably realistic description of the interaction between liquid-crystal molecules. It is based on an ansatz suggested by Berne and Pechukas [25], who realized that the anisotropy of the interaction of two rodlike molecules can be approximated by the convolution of two ellipsoidal Gaussians. Mathematically the convolution yields another Gaussian characterized by a standard deviation $\sigma_{ff}(\hat{\mathbf{r}}_{ij},\hat{\mathbf{u}}_i,\hat{\mathbf{u}}_j)$ where $\hat{\mathbf{r}}_{ij}$ is a unit vector in the direction of the center-of-mass distance vector $\mathbf{r}_{ij}$ and $\hat{\mathbf{u}}_i$, $\hat{\mathbf{u}}_j$ are unit vectors (so-called microscopic directors) specifying the orientation of film molecules with respect to a space-fixed coordinate system. Using $\sigma_{ff}(\hat{\mathbf{r}}_{ij},\hat{\mathbf{u}}_i,\hat{\mathbf{u}}_j)$ Gay and Berne [19] proposed a modified Lennard-Jones (12,6) potential for ellipsoids of revolution:

$$\begin{aligned} u_{ff}(\mathbf{r}_{ij},\hat{\mathbf{u}}_i,\hat{\mathbf{u}}_j) &= 4\epsilon_{ff}(\hat{\mathbf{r}}_{ij},\hat{\mathbf{u}}_i,\hat{\mathbf{u}}_j) \\ &\times\left[\left(\frac{\sigma_{ff}^s}{r_{ij}-\sigma_{ff}(\hat{\mathbf{r}}_{ij},\hat{\mathbf{u}}_i,\hat{\mathbf{u}}_j)+\sigma_{ff}^s}\right)^{12}\right. \\ &\left.-\left(\frac{\sigma_{ff}^s}{r_{ij}-\sigma_{ff}(\hat{\mathbf{r}}_{ij},\hat{\mathbf{u}}_i,\hat{\mathbf{u}}_j)+\sigma_{ff}^s}\right)^{6}\right], \end{aligned} \tag{4}$$

where

$$\begin{aligned} \sigma_{ff}(\hat{\mathbf{r}}_{ij},\hat{\mathbf{u}}_i,\hat{\mathbf{u}}_j) &= \sigma_{ff}^s\left\{1-\frac{\chi}{2}\left[\frac{(\hat{\mathbf{r}}_{ij}\cdot\hat{\mathbf{u}}_i+\hat{\mathbf{r}}_{ij}\cdot\hat{\mathbf{u}}_j)^2}{1+\chi\hat{\mathbf{u}}_i\cdot\hat{\mathbf{u}}_j}\right.\right. \\ &\left.\left.+\frac{(\hat{\mathbf{r}}_{ij}\cdot\hat{\mathbf{u}}_i-\hat{\mathbf{r}}_{ij}\cdot\hat{\mathbf{u}}_j)^2}{1-\chi\hat{\mathbf{u}}_i\cdot\hat{\mathbf{u}}_j}\right]\right\}^{-1/2}, \end{aligned} \tag{5}$$

$$\chi := \frac{(\sigma_{ff}^e/\sigma_{ff}^s)^2-1}{(\sigma_{ff}^e/\sigma_{ff}^s)^2+1} = \frac{\kappa_{ff}^2-1}{\kappa_{ff}^2+1}, \tag{6}$$

and σ_{ff}^e and σ_{ff}^s are the zeros of u_{ff} for end-end configurations (i.e., $\hat{\mathbf{r}}_{ij}\|\hat{\mathbf{u}}_i\|\hat{\mathbf{u}}_j$) and side-side configurations ($\hat{\mathbf{r}}_{ij}\perp\hat{\mathbf{u}}_i\|\hat{\mathbf{u}}_j$) of two ellipsoidal molecules. The function $\epsilon_{ff}(\hat{\mathbf{r}}_{ij},\hat{\mathbf{u}}_i,\hat{\mathbf{u}}_j)$ is defined in a similar fashion as

$$\begin{aligned} \epsilon_{ff}(\hat{\mathbf{r}}_{ij},\hat{\mathbf{u}}_i,\hat{\mathbf{u}}_j) &= \epsilon_{ff}^s\left\{1-\frac{\chi'}{2}\left[\frac{(\hat{\mathbf{r}}_{ij}\cdot\hat{\mathbf{u}}_i+\hat{\mathbf{r}}_{ij}\cdot\hat{\mathbf{u}}_j)^2}{1+\chi'\hat{\mathbf{u}}_i\cdot\hat{\mathbf{u}}_j}\right.\right. \\ &\left.\left.+\frac{(\hat{\mathbf{r}}_{ij}\cdot\hat{\mathbf{u}}_i-\hat{\mathbf{r}}_{ij}\cdot\hat{\mathbf{u}}_j)^2}{1-\chi'\hat{\mathbf{u}}_i\cdot\hat{\mathbf{u}}_j}\right]\right\}^2[1-\chi^2(\hat{\mathbf{u}}_i\cdot\hat{\mathbf{u}}_j)^2]^{-1/2}, \end{aligned} \tag{7}$$

where

$$\chi' := \frac{\sqrt{\epsilon_{ff}^s/\epsilon_{ff}^e}-1}{\sqrt{\epsilon_{ff}^s/\epsilon_{ff}^e}+1} = \frac{\sqrt{\kappa_{ff}'}-1}{\sqrt{\kappa_{ff}'}+1} \tag{8}$$

and $\kappa_{ff}'=\epsilon_{ff}^s/\epsilon_{ff}^e$ denotes the ratio of the potential well depths for side-side and end-end configurations. The values σ_{ff}^s and ϵ_{ff}^s are used to express all quantities in the customary dimensionless (starred) units [26].

The interaction between ellipsoidal film molecules and spherical wall atoms is modeled by analogy with the Gay-Berne potential as

$$\begin{aligned} u_{fw}^{(k)} &= 4\epsilon_{fw}(\hat{\mathbf{r}}_{ij}^{(k)},\hat{\mathbf{u}}_j)\left[\left(\frac{\sigma_{fw}^s}{r_{ij}^{(k)}-\sigma_{fw}(\hat{\mathbf{r}}_{ij}^{(k)},\hat{\mathbf{u}}_j)+\sigma_{fw}^s}\right)^{12}\right. \\ &\left.-\left(\frac{\sigma_{fw}^s}{r_{ij}^{(k)}-\sigma_{fw}(\hat{\mathbf{r}}_{ij}^{(k)},\hat{\mathbf{u}}_j)+\sigma_{fw}^s}\right)^{6}\right], \end{aligned} \tag{9}$$

where $\hat{\mathbf{r}}_{ij}^{(k)}$ is a unit vector in the direction of the distance vector $\mathbf{r}_{ij}^{(k)}$ between an atom in wall k and the center of mass of a film molecule and $r_{ij}^{(k)}=\|\mathbf{r}_{ij}^{(k)}\|$. In Eq. (9) $\sigma_{fw}(\hat{\mathbf{r}}_{ij}^{(k)},\hat{\mathbf{u}}_j)$ is the standard deviation of a Gaussian obtained from a similar convolution of a spherical and an ellipsoidal Gaussian which can be written explicitly as

$$\sigma_{fw}(\hat{\mathbf{r}}_{ij}^{(k)},\hat{\mathbf{u}}_j) = \sigma_{fw}^s[1-a(\hat{\mathbf{r}}_{ij}^{(k)}\cdot\hat{\mathbf{u}}_j)^2]^{-1/2}, \tag{10a}$$

with

$$a := 1-(\kappa_{fw})^{-2} = 1-\left(\frac{\sigma_{fw}^e}{\sigma_{fw}^s}\right)^{-2}, \tag{10b}$$

where σ_{fw}^s and σ_{fw}^e are the zeros of u_{fw} for $\hat{\mathbf{r}}_{ij}^{(k)}\perp\hat{\mathbf{u}}_j$ and $\hat{\mathbf{r}}_{ij}^{(k)}\|\hat{\mathbf{u}}_j$, respectively. To obtain an expression for

$\epsilon_{fw}(\hat{\boldsymbol{r}}_{ij}^{(k)},\hat{\boldsymbol{u}}_j)$ one notes the similarity between its counterpart $\epsilon_{ff}(\hat{\boldsymbol{r}}_{ij},\hat{\boldsymbol{u}}_i,\hat{\boldsymbol{u}}_j)$ in Eq. (7) and $\sigma_{ff}(\hat{\boldsymbol{r}}_{ij},\hat{\boldsymbol{u}}_i,\hat{\boldsymbol{u}}_j)$ in Eq. (5). The main difference between the latter two concerns a factor $\propto\hat{\boldsymbol{u}}_i\cdot\hat{\boldsymbol{u}}_j$ in Eq. (7) which has no equivalent in $\epsilon_{fw}(\hat{\boldsymbol{r}}_{ij}^{(k)},\hat{\boldsymbol{u}}_j)$ because wall atoms are spherical. Under this proviso and by analogy with Eqs. (5) and (7) we have from Eq. (10a)

$$\epsilon_{fw}(\hat{\boldsymbol{r}}_{ij},\hat{\boldsymbol{u}}_j)=\epsilon_{fw}^{s}[1-a'(\hat{\boldsymbol{r}}_{ij}^{(k)}\cdot\hat{\boldsymbol{u}}_j)^2]^2, \tag{11a}$$

where

$$a':=1-(\kappa_{fw}')^{-1/2}=1-\left(\frac{\epsilon_{fw}^{s}}{\epsilon_{fw}^{e}}\right)^{-1/2} \tag{11b}$$

and ϵ_{fw}^{e}, ϵ_{fw}^{s} denote the depths of potential wells for sphere-end and sphere-side configurations, respectively. At this point the set of parameters $\{\sigma_{fw}^{e},\sigma_{fw}^{s},\epsilon_{fw}^{e},\epsilon_{fw}^{s}\}$ governing the fluid-wall interaction potential is yet undetermined. A particular choice of values employed in this work will be rationalized subsequently in Sec. III B where we emphasize technical aspects of our GCEMC simulation.

III. THEORETICAL BACKGROUND

A. Statistical-physical description of confined liquid-crystal films

For a film confined between discrete walls and open to a bulk fluid reservoir in the thermodynamic sense, it was shown in [27] that the exact differential of the grand potential, which governs infinitesimal, reversible transformations in an open system, can be written as

$$d\Omega=-SdT-Nd\mu+\gamma' dA+T_{zz}Ads_z, \tag{12}$$

where $\{T,\mu,A,s_z\}$ is the set of natural variables. The expression in Eq. (12) explicitly assumes that the walls are in registry [cf. Eq. (1)] and that the film is not sheared. In Eq. (12) S denotes entropy, γ' is a film-wall interfacial tension, A is the area of film-wall contact, and T_{zz} is the average stress applied normally to A. By convention, T_{zz} is negative if the force exerted by the film on the wall points outward. From Eq. (12) it immediately follows that

$$AT_{zz}=\left(\frac{\partial\Omega}{\partial s_z}\right)_{T,\mu,A}, \tag{13}$$

which is of interest here because this stress tensor element can be measured in principle in complementary SFA experiments. A molecular expression for T_{zz} can be derived from Eq. (13) and

$$\Omega=-k_BT\ln\Xi, \tag{14}$$

which follows from standard textbook considerations (k_B Boltzmann's constant) [28]. The grand canonical partition function Ξ can be expressed as

$$\Xi(\mu,T,s_z,A)=\sum_{N=0}^{\infty}\exp(\mu N/k_BT)Q_N(T,s_z,A). \tag{15}$$

In Eq. (15) Q_N is the canonical partition function. For a molecular system like a liquid crystal it can be cast as

$$Q_N=\frac{1}{N!h^{5N}}\int\exp[-\beta H(\boldsymbol{r}^N,\boldsymbol{p}^N,\boldsymbol{\omega}^N,\boldsymbol{p}_{\boldsymbol{\omega}}^N)]d\boldsymbol{r}^N d\boldsymbol{p}^N d\boldsymbol{\omega}^N d\boldsymbol{p}_{\boldsymbol{\omega}}^N \tag{16}$$

in the classical limit where $\beta:=(k_BT)^{-1}$, $\boldsymbol{p}^N=\{\boldsymbol{p}_1,\boldsymbol{p}_2,\ldots,\boldsymbol{p}_N\}$ are the momenta conjugate to the center-of-mass positions $\boldsymbol{r}^N=\{\boldsymbol{r}_1,\boldsymbol{r}_2,\ldots,\boldsymbol{r}_N\}$, $\boldsymbol{\omega}^N=\{\boldsymbol{\omega}_1,\boldsymbol{\omega}_2,\ldots,\boldsymbol{\omega}_N\}$ are Euler angles specifying molecular orientations [$\boldsymbol{\omega}_i=(\theta_i,\phi_i)$ for linear molecules], $\boldsymbol{p}_{\boldsymbol{\omega}}^N=\{\boldsymbol{p}_{\boldsymbol{\omega}_1},\boldsymbol{p}_{\boldsymbol{\omega}_2},\ldots,\boldsymbol{p}_{\boldsymbol{\omega}_N}\}$ are the momenta conjugate to $\boldsymbol{\omega}^N$, and h is Planck's constant. The exponent 5 in Eq. (16) takes notice of the five degrees of freedom (three translational and two rotational) of the ellipsoidal Gay-Berne molecules. The Hamiltonian

$$H=\sum_{i=1}^{N}\frac{\boldsymbol{p}_i^2}{2m}+\sum_{i=1}^{N}\sum_{\alpha=x,y}\frac{L_{i\alpha}^2}{I}+U(\boldsymbol{r}^N,\boldsymbol{\omega}^N) \tag{17}$$

is split into translational and rotational kinetic contributions and the intermolecular potential $U(\boldsymbol{r}^N,\boldsymbol{\omega}^N)$. In Eq. (17) $L_{i\alpha}$ is the component of the angular momentum referred to the body-fixed principal axis α of molecule i, I is the (scalar) moment of inertia, and m is the molecular mass. For a system without rotational degrees of freedom a division of the Hamiltonian into kinetic and potential contributions immediately leads to a factorization of Q_N into a kinetic part and the configurational integral because in a classical equilibrium system momenta are independent of each other and of $\boldsymbol{r}^N$. For a system with rotational degrees of freedom, on the other hand, Gray and Gubbins point out that $\boldsymbol{L}^N=\boldsymbol{L}^N(\boldsymbol{\omega}^N,\boldsymbol{p}_{\boldsymbol{\omega}}^N)$ so that a similar factorization is prevented [29]. The factorization of Q_N is, however, possible if one introduces the transformation $\boldsymbol{p}_{\boldsymbol{\omega}}^N\rightarrow\boldsymbol{L}^N$. This permits one to rewrite Eq. (16) as

$$Q_N=\frac{1}{N!h^{5N}}\int\exp[-\beta H(\boldsymbol{r}^N,\boldsymbol{p}^N,\boldsymbol{\omega}^N,\boldsymbol{p}_{\boldsymbol{\omega}}^N)]\times d\boldsymbol{r}^N d\boldsymbol{p}^N d\boldsymbol{\omega}^N|J^{(N)}|d\boldsymbol{L}^N, \tag{18}$$

where $|J^{(N)}|$ is the absolute value of the Jacobian of this transformation. Since $\boldsymbol{L}_i$ is independent of $\boldsymbol{p}_{\boldsymbol{\omega}_j}$ for $i\neq j$, $J^{(N)}=J_1J_2\cdots J_N$ where J_i is given by

$$J_i:=\frac{\partial(p_{\phi_i}p_{\theta_i})}{\partial(L_{x_i}L_{y_i})}=-\sin\theta_i. \tag{19}$$

Introducing Eq. (19) together with

$$\sin\theta_i d\theta_i d\phi_i=d\hat{\boldsymbol{u}}_i\quad(i=1,\ldots,N) \tag{20}$$

eventually permits one to rewrite Eq. (18) as

$$Q_N=Q_{\text{trans}}Q_{\text{rot}}\widetilde{Z}_N, \tag{21}$$

where

$$\widetilde{Z}_N=\frac{1}{N!2^N}\int\exp[-\beta U]d\boldsymbol{r}^N d\hat{\boldsymbol{u}}^N=\frac{1}{N!2^N}Z_N. \tag{22}$$

In Eq. (22) Z_N denotes the configurational integral, the extra factor 2^{-N} corrects for double counting equivalent orientations $\hat{\boldsymbol{u}}_i$ and $-\hat{\boldsymbol{u}}_i$. In Eq. (21) $Q_{\rm trans}$ and $Q_{\rm rot}$ represent integrals over momentum and angular momentum space which can be carried out analytically to give

$$Q_{\rm trans}=\left(\frac{2\pi m}{\beta h^2}\right)^{3N/2}=:\Lambda^{-3N},$$

$$Q_{\rm rot}=\left(\frac{2\pi I}{\beta h^2}\right)^{N}=\Lambda^{-2N}\left(\frac{I}{m}\right)^{N}, \tag{23}$$

where Λ is the thermal de Broglie wavelength [28]. Combining now Eqs. (21)–(23) and inserting the resulting expression into Eq. (15) permits one to reexpress the grand canonical partition function in factorized form as

$$\Xi(\mu,T,s_z,A)=\sum_{N=0}^{\infty}\frac{\Lambda^{-5N}}{N!}\left(\frac{I}{2m}\right)^{N}\times\exp(\mu N/k_BT)Z_N(T,s_z,A). \tag{24}$$

From Eqs. (13), (14), and (24) one obtains a molecular expression for T_{zz}, namely,

$$\begin{aligned}AT_{zz}&=\left(\frac{\partial\Omega}{\partial s_z}\right)_{T,\mu,A}\\&=-k_BT\left(\frac{\partial\ln\Xi}{\partial s_z}\right)_{T,\mu,A}\\&=-\frac{k_BT}{\Xi}\sum_{N=0}^{\infty}\frac{\Lambda^{-5N}}{N!}\left(\frac{I}{2m}\right)^{N}\exp(\mu N/k_BT)\left(\frac{\partial Z_N}{\partial s_z}\right)_{T,\mu,A}.\end{aligned} \tag{25}$$

Depending on how the partial derivative of Z_N is evaluated, two alternative forms for T_{zz} obtain. This is demonstrated by writing more explicitly

$$\frac{\partial Z_N}{\partial s_z}=\frac{\partial}{\partial s_z}\prod_{i=1}^{N}\int d\hat{\boldsymbol{u}}_i\int_0^s dx_i\int_0^s dy_i\int_0^{s_z}dz_i\times\exp[-\beta U(\boldsymbol{r}^N,\hat{\boldsymbol{u}}^N)]. \tag{26}$$

In Eq. (26) s_z appears as a variable in the upper limit of the fourth integral as well as in the argument of U because of the contribution $U_{FW}^{(2)}$ [cf. Eq. (2)] which contains s_z as an argument via

$$r_{ij}^{(2)}=[(x_i-x_j^{(2)})^2+(y_i-y_j^{(2)})^2+(z_i-s_z)^2]^{1/2} \tag{27}$$

because of Eq. (1). Applying Leibniz's rule for the differentiation of an integral [30] therefore yields

$$\frac{\partial Z_N}{\partial s_z}=-\frac{1}{k_BT}\prod_{i=1}^{N}\int d\hat{\boldsymbol{u}}_i\int_0^s dx_i\int_0^s dy_i\int_0^{s_z}dz_i\frac{\partial U_{FW}^{(2)}}{\partial s_z}\times e^{-\beta U(\boldsymbol{r}^N,\hat{\boldsymbol{u}}^N)}. \tag{28}$$

The contributions from the upper limits on the integrations over z_i vanish, since U becomes infinite at $z_i=s_z$ on account of the implicit hard-wall background [see Eqs. (2), (3)]. More explicitly,

$$\frac{\partial U_{FW}^{(2)}}{\partial s_z}=-\sum_{i=1}^{N}\sum_{j=1}^{N_s}\frac{du_{fw}^{(2)}}{dr_{ij}^{(2)}}\frac{z_i-s_z}{r_{ij}^{(2)}}=\sum_{i=1}^{N}\sum_{j=1}^{N_s}F_{z,ij}^{(2)}=F_z^{(2)}, \tag{29}$$

where $F_{z,ij}^{(2)}$ is the z component of the force exerted by atom j in wall 2 on the center of mass of film molecule i. Inserting now Eqs. (26), (28), and (29) into Eq. (25) yields

$$\begin{aligned}T_{zz}&=\frac{1}{A\Xi}\sum_{N=0}^{\infty}\frac{\Lambda^{-5N}}{N!}\left(\frac{I}{2m}\right)^{N}\exp(\mu N/k_BT)\\&\quad\times\int d\hat{\boldsymbol{u}}^N\int d\boldsymbol{r}^N F_z^{(2)}\exp[-\beta U(\boldsymbol{r}^N,\hat{\boldsymbol{u}}^N)]\\&=\frac{1}{A}\sum_{N=0}^{\infty}\int d\hat{\boldsymbol{u}}^N\int d\boldsymbol{r}^N F_z^{(2)}f_{\mu VT}=\frac{\langle F_z^{(2)}\rangle}{A},\end{aligned} \tag{30}$$

which introduces the probability density function $f_{\mu VT}$ of the grand canonical ensemble and expresses T_{zz} as an ensemble average of the z component of the net force per unit area exerted by the upper wall (2) on the film. This force must be applied externally in order to keep wall (2) stationary in the state of thermodynamic equilibrium. Likewise, $\langle F_z^{(2)}\rangle$ may be viewed as the z component of the negative total force per unit area exerted by the film on the wall. Because of mechanical stability,

$$\langle F_z^{(2)}\rangle=-\langle F_z^{(1)}\rangle. \tag{31}$$

On account of its functional form, Eq. (30)—together with Eq. (31)—is termed the ''force'' expression for T_{zz}. An alternative expression can be derived by transforming variables according to

$$\begin{aligned}z_i\rightarrow\tilde{z}_i&=z_is_z^{-1}\quad(i=1,\ldots,N),\\z_i^{(k)}\rightarrow\tilde{z}_i^{(k)}&=z_i^{(k)}s_z^{-1}\quad(i=1,\ldots,N_s;k=1,2)\end{aligned} \tag{32}$$

so that Eq. (26) reads

$$\frac{\partial Z_N}{\partial s_z}=\frac{\partial}{\partial s_z}s_z^N\prod_{i=1}^{N}\int d\hat{\boldsymbol{u}}_i\int_0^s dx_i\int_0^s dy_i\int_0^1 d\tilde{z}_i\exp(-\beta U). \tag{33}$$

Scaling affects both U_{FF} and $U_{FW}^{(k)}$ because of

$$\begin{aligned}r_{ij}&=[(x_i-x_j)^2+(y_i-y_j)^2+s_z^2(\tilde{z}_i-\tilde{z}_j)^2]^{1/2},\\r_{ij}^{(k)}&=[(x_i-x_j^{(k)})^2+(y_i-y_j^{(k)})^2+s_z^2(\tilde{z}_i-\tilde{z}_j^{(k)})^2]^{1/2},\end{aligned} \tag{34}$$

and the differentiation gives

$$\frac{\partial Z_N}{\partial s_z}=\frac{NZ_N}{s_z}-\frac{\beta}{s_z}\prod_{i=1}^{N}\int d\hat{\boldsymbol{u}}_i\int_0^s dx_i\int_0^s dy_i\int_0^{s_z}dz_iW_{zz}\times\exp(-\beta U), \tag{35}$$

after reverting the transformation [Eqs. (32)]. In Eq. (35) W_{zz} is defined as

$$W_{zz} := \frac{1}{2}\sum_{i=1}^{N}\sum_{j\neq i}^{N}\frac{du_{ff}}{dr_{ij}}\frac{z_{ij}^2}{r_{ij}} + \sum_{k=1}^{2}\sum_{i=1}^{N}\sum_{j=1}^{N_s}\frac{du_{fw}^{(k)}}{dr_{ij}^{(k)}}\frac{[z_{ij}^{(k)}]^2}{r_{ij}^{(k)}} =: W_{zz}^{FF} + W_{zz}^{FW}, \tag{36}$$

where $z_{ij} := z_i - z_j$ and $z_{ij}^{(k)} := z_i - z_j^{(k)}$. Inserting Eq. (35) into Eq. (25) gives

$$T_{zz} = T_{zz}^{FF} + T_{zz}^{FW}, \tag{37a}$$

where

$$T_{zz}^{FF} = -\frac{\langle N\rangle k_B T}{As_z} + \frac{1}{As_z}\sum_{N=0}^{\infty}\int d\hat{\boldsymbol{u}}^N \int d\boldsymbol{r}^N W_{zz}^{FF} f_{\mu VT} = -\frac{\langle N\rangle k_B T}{As_z} + \frac{\langle W_{zz}^{FF}\rangle}{As_z}, \tag{37b}$$

$$T_{zz}^{FW} = \frac{1}{As_z}\sum_{N=0}^{\infty}\int d\hat{\boldsymbol{u}}^N \int d\boldsymbol{r}^N W_{zz}^{FW} f_{\mu VT} = \frac{\langle W_{zz}^{FW}\rangle}{As_z}. \tag{37c}$$

Because of Eq. (36) Eqs. (37) will henceforth be called the ''virial'' form of T_{zz}. Similar virial and force expressions have been derived previously [31,32] for ''simple'' films. In [31] the film was confined between rigid discrete walls similar to the ones employed here whereas in [32] these walls were thermally coupled to the film via the Einstein model of a crystal. The expressions in Eqs. (30) and (37) differ from their counterparts in [31] by an additional integration over molecular orientation due to the rotational degrees of freedom of our molecules. They also lack additional mean-field contributions which arise in [32] because of the Einstein model. Despite these details force and virial forms provide a useful check on internal consistency of computer simulations. This is demonstrated in [31,32] for various ensembles and different thermodynamic states and holds for the present model, too.

B. Grand canonical Monte Carlo method

Unfortunately none of the expressions for T_{zz} just derived can be solved analytically for the present model. Thus we resort to GCEMC simulations which provide a numerical route to this quantity. In GCEMC generation of a (numerical representation of a) Markov chain of configurations proceeds in two consecutive steps. In the first step one of the N molecules, say i, is chosen at random and its center of mass is displaced slightly within a small cube of side length $2d_{\max}$ centered on its original position $\boldsymbol{r}_i^{[k]}$, that is,

$$\boldsymbol{r}_i^{[l]} = \boldsymbol{r}_i^{[k]} + d_{\max}(\mathbf{1} - 2\boldsymbol{\xi}), \tag{38}$$

where the superscripts refer to original $[k]$ and new trial configuration $[l]$, $\mathbf{1}=(1,1,1)$ and $\boldsymbol{\xi}$ is a vector whose three components are pseudorandom numbers distributed uniformly on the interval $[0,1]$. Then one of the three axes of the Cartesian coordinate system is chosen at random and the molecule is rotated randomly by a small angle increment

$$\Delta\psi_{k\to l} = \psi_{\max}(1 - 2\xi) \tag{39}$$

around that axis. Both $d_{\max}$ and $\psi_{\max}$ are adjusted during a run to preserve an acceptance ratio of 40–60 % of displacement and rotation attempts. From the theory of Markov processes [33] it follows that the probability for the transition $k\to l$ is governed by the ratio $f_{\mu VT}^{[l]}/f_{\mu VT}^{[k]}$ where from Eq. (30)

$$f_{\mu VT} \propto \exp\left[-\beta(U-\mu N) - \ln N! - N\ln\left(\frac{2m\Lambda^5}{VI}\right)\right] \tag{40}$$

after a convenient transformation

$$\boldsymbol{r}^N \to \tilde{\boldsymbol{r}}^N = \{x_1/s, y_1/s, z_1/s_z, \ldots, x_N/s, y_N/s, z_N/s_z\}$$

which gives rise to the term $\propto N\ \ln V$ in Eq. (40) [26]. Since N does not vary during the first step, it is easy to verify that

$$\frac{f_{\mu VT}^{[l]}}{f_{\mu VT}^{[k]}} = \exp[-\beta\Delta U_{k\to l}], \tag{41}$$

where $\Delta U_{k\to l}$ is the change in configurational energy associated with displacement and rotation of molecule i. Employing Metropolis's algorithm [26] the transition $k\to l$ is accepted with a probability

$$p_1 = \min\{1, \exp(-\beta\Delta U_{k\to l})\} \tag{42}$$

in the usual way. During the second step an attempt is made to alter N by either adding or removing one film molecule in an unbiased way, that is, $\Delta N_{k\to l} := N^{[l]} - N^{[k]} = \pm 1$. Addition and removal are attempted with equal probability. If $\Delta N_{k\to l} = +1$ a new molecule is added from a virtual reservoir of matter with random orientation at a randomly selected position in V; if $\Delta N_{k\to l} = -1$ an already existing molecule is chosen at random and subjected to a removal attempt. Addition and removal attempts are accepted on the basis of a *modified* Metropolis criterion

$$p_2 = \min\{1, f_{\mu VT}^{[l]}/f_{\mu VT}^{[k]} = \exp(r_{k\to l})\}, \tag{43}$$

where the argument of the pseudo Boltzmann factor is given by

$$r_{k\to l} = -\ln N^{[l]} - \beta\Delta U^{[l]} + \tilde{B} \tag{44a}$$

for addition $(\Delta N_{k\to l} = +1)$ and by

$$r_{k\to l} = \ln N^{[k]} + \beta\Delta U^{[k]} - \tilde{B} \tag{44b}$$

for removal $(\Delta N_{k\to l} = -1)$. In Eqs. (44) $\Delta U^{[k]}$ and $\Delta U^{[l]}$ denote configurational energy differences due to the additional molecule in the old $[k]$ and the new trial configuration $[l]$, respectively. The dimensionless constant

$$\tilde{B} = \beta\mu - \ln\left(\frac{2m\Lambda^5}{VI}\right) \tag{45}$$

depends on the thermodynamic state via the set $\{\mu, V, T\}$, molecular mass m, and the moment of inertia I which can be cast analytically as

TABLE I. Technical details of the GCEMC simulations.

Temperature T^*	1.25
Thermal de Broglie wavelength for given temperature, Λ^*	0.0663
Chemical potential μ^*	-10.1 (film); $-10.1, -8.1, -7.1$ (bulk)
Lattice constant of the fcc (100) walls, l^*	1.90
Side length of simulation cell in the x-y plane, s^*	11.422
Axis ratio of fluid molecules κ_{ff}	3.0
Ratio of potential well depths (u_{ff}), κ'_{ff}	5.0
Potential well depth of u_{fw} for $\hat{\mathbf{u}}_i \perp \hat{\mathbf{r}}_{ij}^{(k)}$, u_{fw}^s	1.0
Ratio of potential well depths (u_{fw}), κ'_{fw}	2.5
Starting configuration	random
Number of equilibration steps	$(1.0-1.5)\times 10^7$
Total number of MC steps	$(2.0-3.0)\times 10^7$
Cutoff radius for fluid-fluid interaction, $(r_{ff}^c)^*$	4.0
Cutoff radius of neighbor list	4.5
Cutoff radius for fluid-wall interaction, $(r_{fw}^c)^*$	3.44
Thickness of imaginary layer used in computation of $\overline{\rho}$ and h, Δz^*	0.05–0.12
Interval of u_z^2 used in computation of h, Δu_z^2	0.05

$$\frac{I}{m}=\frac{1}{20}(\sigma_{ff}^s)^2(1+\kappa_{ff}^2) \tag{46}$$

for ellipsoids of revolution.

Out of convenience we introduce a potential cutoff (see Table I) and modify u_{ff} and u_{fw} so that both potentials vanish identically at intermolecular separations equal to or larger than this cutoff. Specifically, we replace u_{ff} in the GCEMC simulations by

$$u_{ff}^{\mathrm{sim}}=\begin{cases} 0, & r_{ij}\geqslant r_{ff}^c \\ \infty, & r_{ij}-\sigma_{ff}(\hat{\mathbf{r}}_{ij},\hat{\mathbf{u}}_i,\hat{\mathbf{u}}_j)+\sigma_{ff}^s\leqslant 0 \\ u_{ff}(\mathbf{r}_{ij},\hat{\mathbf{u}}_i,\hat{\mathbf{u}}_j)-u_{ff}(r_{ff}^c\hat{\mathbf{r}}_{ij},\hat{\mathbf{u}}_i,\hat{\mathbf{u}}_j), & \text{otherwise,} \end{cases} \tag{47}$$

where $r_{ff}^c:=\sigma_{ff}^e+\sigma_{ff}^s$. We note in passing that u_{ff}^{sim} is set to infinity if the denominators in Eq. (4) become negative. This is necessary because the Gay-Berne potential [Eq. (4)] has an unphysical minimum for strongly overlapping configurations of a molecule pair, a deficiency of the Gay-Berne potential which is due to $\sigma_{ff}(\hat{\mathbf{r}}_{ij},\hat{\mathbf{u}}_i,\hat{\mathbf{u}}_j)$ and rarely discussed in the literature. It obviously leads to nonsensical results especially in simulations involving particle insertions but may also affect complementary approaches based on, say, density functional theory or integral equations if the limits of integration are chosen improperly. The fluid-wall potential is modified the same way and replaced by u_{fw}^{sim} which involves, however, $\sigma_{fw}(\hat{\mathbf{r}}_{ij},\hat{\mathbf{u}}_j)$ and $r_{fw}^c:=\sigma_{fw}^e+\sigma_{fw}^s$ instead of $\sigma_{ff}(\hat{\mathbf{r}}_{ij},\hat{\mathbf{u}}_i,\hat{\mathbf{u}}_j)$ and r_{ff}^c in Eq. (47). Because u_{ff}^{sim} and u_{fw}^{sim} are short-range potentials we employ minimum image convention and periodic boundary conditions in all three (x,y,z; bulk phase) or two (x,y; confined film) dimensions [26].

All results presented below are obtained for $\kappa_{ff}=3$ and $\kappa'_{ff}=5$. From Eqs. (5)–(8) one notes that in reduced units (see above) $\sigma_{ff}(\hat{\mathbf{r}}_{ij},\hat{\mathbf{u}}_i,\hat{\mathbf{u}}_j)$ and $\epsilon_{ff}(\hat{\mathbf{r}}_{ij},\hat{\mathbf{u}}_i,\hat{\mathbf{u}}_j)$ are completely determined once κ_{ff} and κ'_{ff} are specified. To determine $\sigma_{fw}(\hat{\mathbf{r}}_{ij},\hat{\mathbf{u}}_j)$ we express the zero of u_{fw} for configurations $\hat{\mathbf{r}}_{ij}\perp\hat{\mathbf{u}}_i$ as

$$\sigma_{fw}^s:=(\sigma_w+\sigma_{ff}^s)/2 \tag{48}$$

for purely geometrical reasons where σ_w denotes the ''diameter'' of a wall atom. In the same spirit we write

$$\sigma_{fw}^e:=(\sigma_w+\sigma_{ff}^e)/2 \tag{49}$$

for configurations $\hat{\mathbf{r}}_{ij}\|\hat{\mathbf{u}}_i$. In addition, equal ''volumes'' for fluid molecules and wall atoms are assumed, so that

$$\sigma_W^3=(\sigma_{ff}^s)^2\sigma_{ff}^e \Rightarrow \sigma_W=\sqrt[3]{3}\sigma_{ff}^s \tag{50}$$

and $\sigma_{fw}(\hat{\mathbf{r}}_{ij}^{(k)},\hat{\mathbf{u}}_j)$ is completely determined. Equations (48)–(50) are, of course, *ad hoc* assumptions but do not seem to be too unreasonable especially in view of the lack of more refined potential models for the interaction between wall atoms and film molecules. However, two undetermined parameters remain, namely, ϵ_{fw}^s and $\kappa'_{fw}=\epsilon_{fw}^s/\epsilon_{fw}^e$ [see Eqs. (11)]. In this article we take $\epsilon_{fw}^s=\epsilon_{ff}^s$ and $\kappa_{fw}=\kappa'_{ff}/2$ favoring an alignment of the microscopic director parallel with the wall. The impact of other choices for $\{\epsilon_{fw}^s,\epsilon_{fw}^e\}$ is planned to be discussed in a separate publication [34].

The simulations were performed with a fully vectorized GCEMC program incorporating neighbor lists on a Cray J932 where a typical run of 10^7 MC steps takes about 70 min of CPU time.

IV. RESULTS

A. Isotropic bulk phase

For the special case $\kappa_{ff}=3$ and $\kappa'_{ff}=5$ the phase diagram of the bulk Gay-Berne fluid was meticulously determined by Chalam *et al.* [22]. It reveals the rich phase behavior typical of a liquid crystal, that is, existence of various mesophases in

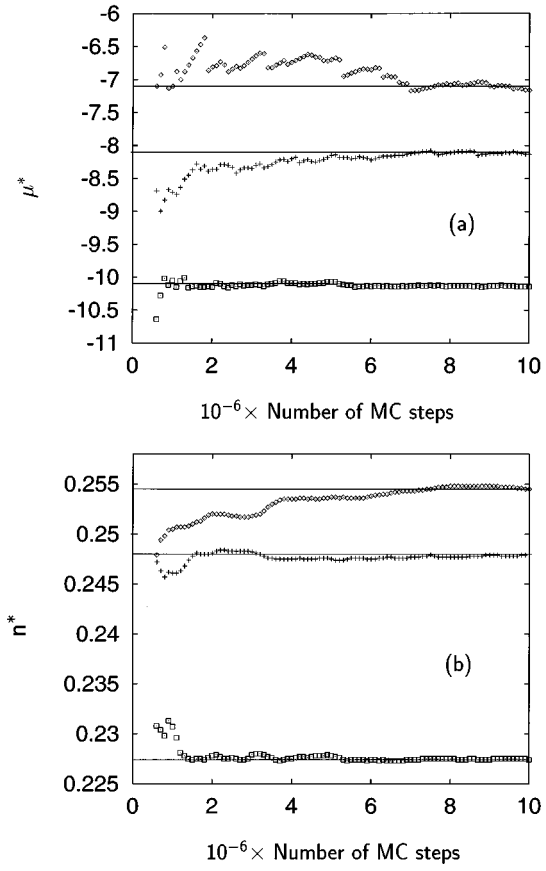

FIG. 1. (a) The chemical potential μ obtained by the test particle method as a function of the number of steps in a canonical ensemble MC simulation at $T^*=1.25$; $n^*=0.2274$ ($\square$), $n^*=0.2480$ ($+$), $n^*=0.2545$ ($\diamond$). (b) The number density $n:=\langle N\rangle/V$ as a function of the number of GCEMC steps at $T^*=1.25$; $\mu^*=-10.1$ ($\square$), $\mu^*=-8.1$ ($+$), $\mu^*=-7.1$ ($\diamond$). The horizontal lines refer to the constant chemical potential of a corresponding GCEMC simulation (a) and to the density employed in a canonical ensemble MC simulation (b), respectively.

addition to an isotropic phase (see Fig. 17 in [22]). Thus for a given temperature T and density n one knows the nature of the phase to which a particular thermodynamic state pertains. If one wants to perform a GCEMC simulation for this very state, however, one does not need its density but the state variable conjugate to it, that is, the chemical potential μ. It can be computed for a given T and n via the test particle method in a MC simulation in the canonical ensemble [35]. If this so-determined μ is utilized in a subsequent GCEMC simulation one can compute the *average* density of the same thermodynamic state now specified uniquely by the set $\{\mu,V,T\}$. Based upon the hypothesis of equivalence of statistical-physical ensembles [36] one expects the *average* density from GCEMC to equal the *fixed* density of the corresponding canonical ensemble MC simulation within statistical accuracy. Applicability of the hypothesis is, however, not guaranteed *a priori* but expected for states characterized by a correlation length sufficiently smaller than the microscopic dimensions of the simulation cell. For three different densities $n^*=0.2274$, 0.2480, 0.2545 and the temperature $T^*=1.25$ we computed μ by the test particle method. These states pertain to the isotropic phase of the Gay-Berne fluid sufficiently off the isotropic-nematic phase transition which at this temperature occurs at $n^*\simeq 0.32$ [22]. Results in Fig. 1(a) show that convergence of the ensemble average, on which the estimated μ is based, depends significantly on n. It is faster at lower n because of the decreasing efficiency with which test particles sample regions of low configurational energy. This is particularly apparent from the discontinuous jumps in the data points for $n^*=0.254$ which disappear gradually with increasing run length, that is, with increasing statistical accuracy. The calculated μ's are then used in GCEMC to determine the average density of a bulk phase at the same temperature T. Results in Fig. 1(b) show that this density converges nicely to the value for which μ was determined in the preceding canonical ensemble MC simulation. Thus for relevant thermodynamic states in this work GCEMC is reliable.

B. Stratification of confined liquid-crystal films

Turning to confined films next, a useful quantitative measure of confinement effects is obtained through the Maxwell relation

$$-\left(\frac{\partial N}{\partial s_z}\right)_{T,\mu,A}=A\left(\frac{\partial T_{zz}}{\partial \mu}\right)_{T,s_z,A}, \tag{51}$$

which follows directly from Eq. (12). Since

$$\lim_{s_z\to\infty} T_{zz}(s_z)=\lim_{s_z\to\infty} T_{zz}^{FF}(s_z)=-P_b \tag{52}$$

the partial differential on the right hand side of Eq. (51) reduces to its bulk counterpart [37]

$$\left(\frac{\partial P_b}{\partial \mu}\right)_{T,V}=n_b \tag{53}$$

in this limit where P_b and n_b denote the pressure and density of a corresponding homogeneous bulk phase, respectively. Thus it proves convenient to introduce

$$r:=\frac{1}{An_b}\left(\frac{\partial\langle N\rangle}{\partial s_z}\right)_{T,\mu,A}\to 1 \quad (s_z\to\infty) \tag{54}$$

as the relative ''rate'' at which the confined film imbibes matter from a (virtual) reservoir as s_z varies with respect to the (constant absolute) bulk imbibition ''rate.'' Because of this definition $r<1$ refers to states for which imbibition is hindered relative to the bulk whereas imbibition is enhanced if $r>1$. The origin of any deviation of r from its bulk value of one must be related to a microscopic structure of the film differing sufficiently from that of a corresponding bulk phase at the same T and μ. Since the thermodynamic state is the same for film and bulk, a different structure of the former can only be induced by the walls so that in this sense r is a direct measure of confinement.

For a thermodynamic state $T^*=1.25$, $\mu^*=-10.1$ to which the remainder of this paper will be restricted we plot r as a function of s_z in Fig. 2. Data points plotted in that figure are obtained by numerically differentiating $\langle N\rangle$ from a sequence of GCEMC simulations at different $\{s_z\}$. As ex-

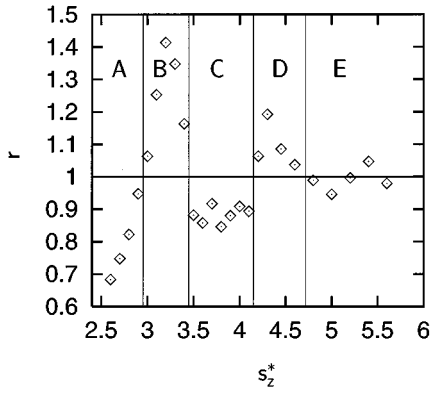

FIG. 2. The relative imbibition ''rate'' r of a confined film with respect to a bulk reservoir at the same temperature T and chemical potential μ as a function of distance between the walls s_z. Zones A–E are identified according to intervals of s_z in which $r>1$ and $r<1$, respectively. Vertical lines separate these zones and the horizontal line demarcates the bulk value $r=1$. Zone E is not divided further because the deviation of r from one is small for $s_z^* \geqslant 4.7$.

pected, r is a damped oscillatory function of s_z which oscillates around the bulk value of one. Intuitively this makes sense because confinement effects are expected to be more pronounced (i.e., the deviation from one is expected to be the larger) the smaller s_z is. Based upon the plot of r in Fig. 2 we divide the range of wall separations studied into different zones depending on whether r is less or greater than one. These zones are demarcated in Fig. 2 by vertical lines. The subsequent discussion of structural aspects will be restricted to representative thermodynamic states (i.e., values of s_z) identified by $s_z^*=2.5$ (zone A), 3.0 and 3.4 (zone B), 4.0 (zone C), 4.5 (zone D), and 5.6 (zone E).

What structural changes are expected as one moves between different zones? From previous work involving films composed of ''simple,'' spherically symmetric molecules it is well known that the most prominent structural feature due to confinement is stratification [7]. This phenomenon is unique in the sense that it is independent of the nature of the fluid-wall interaction potential and occurs whether or not these walls are hard [38] or soft [39], structured or smooth [8]. One is therefore tempted to assume stratification to operate in films consisting of complex fluids, too. A direct measure of stratification is the local density (cf. Sec. I) defined as

$$\overline{\rho}(z;s_z) := \frac{\langle N(z;s_z)\rangle}{A\Delta z}, \tag{55}$$

where $\langle N(z;s_z)\rangle$ is the average number of film molecules located in a thin slice of width Δz (see Table I) centered on z and parallel with the walls. We note that *in general* the local density $\rho(\boldsymbol{r},\boldsymbol{\omega};s_z)$ is a function of molecular orientation $\boldsymbol{\omega}$ because of the anisotropy of film molecules and of (vector) position $\boldsymbol{r}$ because of the corrugation of the walls in transverse directions. However, since we are mainly concerned with stratification for the time being, it seems permissible to average $\rho(\boldsymbol{r},\boldsymbol{\omega};s_z)$ over the x-y plane and to integrate it over all orientations. The result of these operations is $\overline{\rho}(z;s_z)$ where we introduce the overbar to emphasize them.

Plots of $\overline{\rho}(z;s_z)$ for various selected states in zones A–E illustrate stratification as s_z varies. Generally speaking, for all the cases presented in Fig. 3 stratification causes the film to be inhomogeneous, that is, its reduced local density depends on z. If s_z is sufficiently small in zone A only a monolayer of liquid-crystal molecules fits which is located in the middle between the walls for energetic reasons. Going to zone B at $s_z^*=3.0$ the contour of $\overline{\rho}(z;s_z)$ changes substantially, which can be seen by comparison of Figs. 3(a) and 3(b): even though the film seemingly consists of a monolayer, its peak height appears to be significantly reduced compared with the curve in Fig. 3(a). The plot of $\overline{\rho}(z;s_z)$ in Fig. 3(b) is also broader and exhibits shoulders not visible in Fig. 3(a). Regardless of s_z similar shoulders are never observed for a film consisting of simple ''molecules'' and must be ascribed to the molecular nature of our model fluid as we will demonstrate in due course (see Sec. IV C). However, before discussing this aspect further we note from the plot in Fig. 3(c) that at the end of zone B the original shoulders have transformed into two rather tall peaks corresponding to two contact strata (i.e., the strata closest to a wall) and a distinctly smaller middle peak. Thus in zone B a trilayer film appears without participation of an intermediate bilayer film unlike for a film of ''simple'' molecules where the number of strata always changes by one at certain characteristic values of s_z [8]. In zone C the film appears to be less stratified than in zone B, which is inferred from the reduced height of contact-stratum peaks and the almost invisible middle-stratum peak in Fig. 3(d). For a ''simple''-fluid film such a ''disappearance'' of formerly (i.e., at lower s_z) already existing strata upon enlarging s_z has not been observed. In zone D the middle stratum reappears even though the height of the contact-stratum peaks in Fig. 3(e) remains largely unaffected. Finally, in zone E the middle stratum breaks up into two geometrically equivalent middle strata distributed symmetrically around the midplane $z=0$ as one would expect on account of the present registration of the (discrete) walls. If, on the other hand, s_z is sufficiently large the structure of a liquid-crystal film resembles that of a corresponding ''simple'' fluid. This can be seen in Fig. 4 where $\overline{\rho}(z;s_z)$ at $s_z^*=12$ exhibits peaks corresponding to three individual strata in the vicinity of each wall if one scrutinizes the plot creatively. The remainder of the cross section between the walls is homogeneous at the density of a bulk Gay-Berne fluid kept at the same T and μ. According to the exposition at the very beginning of the paper, this is expected at sufficiently large s_z. Homogeneity of the cross section is, of course, a consequence of the particular thermodynamic state which belongs to the isotropic phase of the bulk Gay-Berne fluid.

C. Orientational effects

From the discussion in the preceding section it is evident that the structure of a confined liquid-crystal film differs from that of a corresponding ''simple''-fluid film in three important aspects.

(1) Stratification is less pronounced, that is, even for very thin films individual strata are spatially less well localized and not resolved [see Figs. 3(c)–3(f)].

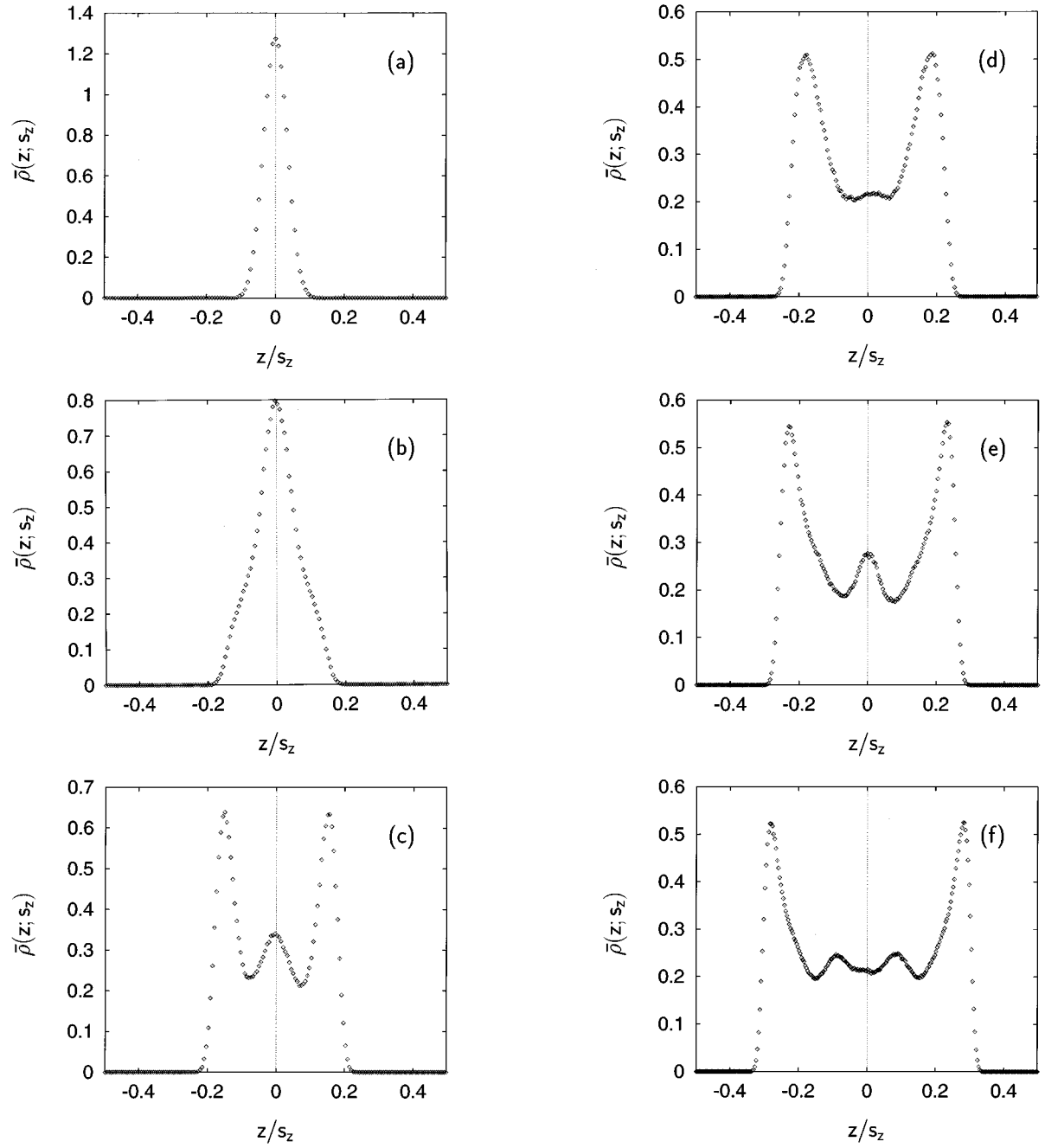

FIG. 3. The reduced local density $\overline{\rho(z;s_z)}$ [see Eq. (55)] as a function of position z/s_z between lower ($z/s_z=-0.5$) and upper ($z/s_z=0.5$) wall. (a) $s_z^*=2.5$ (zone A), (b) $s_z^*=3.0$ (zone B), (c) $s_z^*=3.4$ (zone B), (d) $s_z^*=4.0$ (zone C), (e) $s_z^*=4.5$ (zone D), (f) $s_z^*=5.6$ (zone E). See Fig. 2 for a definition of zones A–E.

(2) In some cases [see, for instance, Fig. 3(b)] stratification begins closer to the walls and not out in the middle (see Fig. 2 in [10]).
(3) Upon enlarging s_z the number of individual strata does not always change by one at certain characteristic values of s_z [see Figs. 3(a)–3(c)].

Thus besides stratification some other mechanism must affect the microscopic structure of a confined liquid-crystal film. Because of the molecules' anisotropy it seems natural to expect orientational effects to be important in this respect. Therefore we introduce the probability of finding a molecule at z with a particular orientation, $f(z,u_z^2;s_z)dzdu_z^2$, where u_z is the cosine of an angle θ between the microscopic director $\hat{\boldsymbol{u}}$ and the z axis. From an operational point of view

$$f(z,u_z^2;s_z)=\frac{\langle N(z,u_z^2;s_z)\rangle}{\langle N\rangle \Delta z \Delta u_z^2}, \tag{56}$$

where $\langle N(z,u_z^2;s_z)\rangle$ is the average number of molecules in a thin slice of width Δz centered on z with an orientation in the interval $[u_z^2-\Delta u_z^2/2,u_z^2+\Delta u_z^2/2]$ (see Table I). The argument u_z^2 (rather than u_z) of the probability density

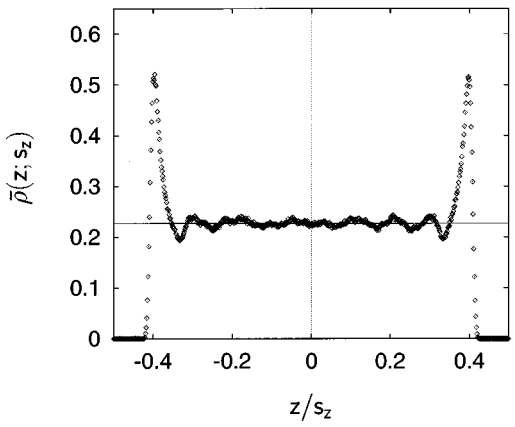

FIG. 4. As Fig. 3 but for $s_z^*=12.0$.

$f(z,u_z^2;s_z)$ takes notice of the nonpolarity of Gay-Berne molecules. On account of its definition, $u_z^2=1.0$ if the microscopic director $\hat{\boldsymbol{u}}$ is parallel with the z axis (i.e., for molecules homeotropically oriented with respect to a wall); $u_z^2=0.0$ if the microscopic director is perpendicular to the z axis (i.e., for molecules lying in planes parallel with the walls). However, $f(z,u_z^2;s_z)$ is not immediately suitable for our purposes which can easily be comprehended by considering a homogenous isotropic phase with no distinguished molecular orientation. One may then write

$$f(z,u_z^2;s_z)du_z^2=f_{\mathrm{iso}}(u_z^2)du_z^2$$
$$=2c\int_0^{2\pi}\int_{\arccos\sqrt{u_z^2}}^{\arccos\sqrt{u_z^2+du_z^2}}\sin\theta\, d\theta\, d\phi$$
$$=\frac{1}{2s_z|u_z|}du_z^2, \tag{57}$$

where the integration is carried out over a spherical layer corresponding to the interval $[u_z^2,u_z^2+du_z^2]$ on the upper hemisphere of the unit sphere. The constant of normalization c is determined such that

$$\int_0^1\int_0^{s_z}f_{\mathrm{iso}}(u_z^2)dz\, du_z^2=1. \tag{58}$$

Thus even though the physics does not distinguish any particular orientation, $f_{\mathrm{iso}}(u_z^2)$ apparently varies in proportion to $|u_z|^{-1}$. It is therefore sensible to introduce a reduced distribution function

$$h(z,u_z^2;s_z):=\frac{f(z,u_z^2;s_z)}{f_{\mathrm{iso}}(u_z^2)}=\frac{2s_z}{\langle N\rangle}\frac{\langle N(z,u_z^2;s_z)\rangle|u_z|}{\Delta z\Delta u_z} \tag{59}$$

as the quantity of prime interest. Clearly, $h(z,u_z^2;s_z)=0$ in spatial regions inaccessible to film molecules (e.g., very close to a wall), $h(z,u_z^2;s_z)=1$ for all $\{z,u_z^2\}$ if the distribution of microscopic directors is isotropic, and $h(z,u_z^2;s_z)\neq 1$ if this is not the case. Plots of $h(z,u_z^2;s_z)$ in Fig. 5 illustrate the orientation of molecules as the film thickens for the same representative states for which $\overline{\rho(z;s_z)}$ is displayed in Fig. 3. In zone A, where the film comprises just a monolayer, the plot in Fig. 5(a) indicates a preferential molecular orientation parallel to the plane of the walls ($u_z^2=0$). Since the hyperplane $h(z,u_z^2;s_z)>0$ over a finite range of orientations, parallel alignment of microscopic directors is not perfect which is, of course, due to thermal motion. In zone B the structure of the film becomes more complex as can be seen from Fig. 5(b) where $h(z,u_z^2;s_z)$ has a bifurcation at small u_z^2 and a maximum at $u_z^2\simeq 0.25$ and $z=0$. Thus in the immediate vicinity of the walls a small fraction of molecules tends to align their microscopic directors parallel with the plane of the wall which is inferred from the double-peak structure at small u_z^2, while the majority of molecules, still located at the center of the film ($z=0$), appear to be tilted with respect to the plane of the wall. The maximum at $u_z^2\simeq 0.25$ corresponds to a tilt angle of $\theta\simeq 60°$ between the microscopic director and the z axis. The double-peak structure in Fig. 5(b) is therefore responsible for the shoulders in $\overline{\rho(z;s_z)}$ discussed previously [see Fig. 3(b)]. At the upper bound of region B the bifurcation has shifted to higher values of u_z^2 and so has the maximum of $h(z=0,u_z^2;s_z)$ in Fig. 5(c) indicating that at the center of the film molecules tend to align their microscopic director more and more parallel with the z axis as space between the walls becomes increasingly available (i.e., with increasing s_z). In the immediate vicinity of the walls molecules prefer a more parallel alignment with the walls as revealed by two well-separated peaks in $h(z,u_z^2;s_z)$ in Fig. 5(c) in the limit $u_z^2\to 0$. Because molecules with a parallel orientation (with respect to a wall) can move closer to that wall due to their cigarlike shape, the two maxima in $h(z,u_z^2;s_z)$ for u_z^2 below the bifurcation move to positions $|z/s_z|$ which are the larger the lower u_z^2 is. In zone C the orientation in the middle layer is rather diffuse but the bifurcation in Fig. 5(d) is still visible and has now moved to even larger u_z^2. The maximum in $h(z=0,u_z^2;s_z)$ is located almost at $u_z^2=1.0$ so that molecules in the middle of the film are perpendicularly oriented with respect to the wall while molecules closer to a wall are aligned in a parallel fashion as one concludes from the two peaks at low u_z^2. A comparison with Fig. 5(e) shows that the orientation in the middle stratum changes from perpendicular (to the plane of the walls) to parallel in zone D: the broad peak in $h(z=0,u_z^2;s_z)$ at high u_z^2 now appears at low u_z^2. In zone D the contact strata are capable of inducing their parallel orientation in the middle layer for the first time. The disappearance of the middle peak of $\overline{\rho(z;s_z)}$ in the sequence of plots in Figs. 3(c)–3(e) is therefore apparently associated with a change in the preferred orientation in the middle layer from tilted [Fig. 5(c)] to perpendicular [Fig. 5(d)] to parallel [Fig. 5(e)]. This effect is due to a competition between preferred orientation and lack of space because of the cigarlike shape of film molecules. Finally, in zone E the middle stratum breaks up into two new strata [Fig. 5(f)] corresponding to molecules which prefer to orient their directors parallel with the plane of the confining walls.

However, in none of these cases do we observe a perfect orientation of molecules in the film. This is particularly apparent from the plots in Fig. 5(e) and Fig. 5(f) which show that molecules in the contact layers can have orientations ranging all the way from parallel to perpendicular (with respect to the wall plane) even though a parallel orientation is

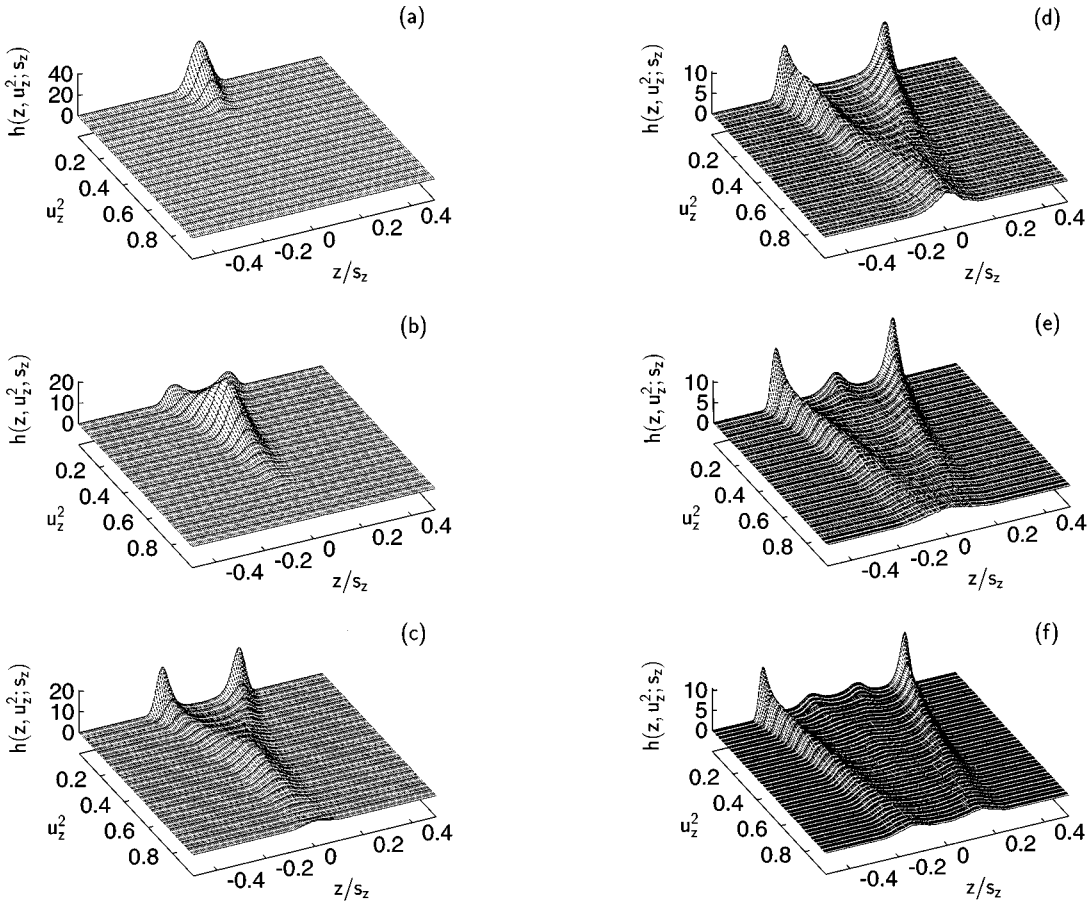

FIG. 5. Density-alignment histogram $h(z,u_z^2;s_z)$ as a function of position z/s_z between lower ($z/s_z=-0.5$) and upper ($z/s_z=0.5$) wall and the squared z component of the microscopic director $\hat{\boldsymbol{u}}$ by which the orientation of film molecules is specified. If $u_z^2=0$, the microscopic director is parallel to the plane of the walls; if $u_z^2=1.0$ the microscopic director is perpendicular to that plane. (a) $s_z^*=2.5$ (zone A), (b) $s_z^*=3.0$ (zone B), (c) $s_z^*=3.4$ (zone B), (d) $s_z^*=4.0$ (zone C), (e) $s_z^*=4.5$ (zone D), (f) $s_z^*=5.6$ (zone E). See Fig. 2 for a definition of zones A–E.

clearly favored because of our choice of film-wall potential parameters. In general, our results for $h(z,u_z^2;s_z)$ show that stratification is less pronounced than in a corresponding ''simple''-fluid film because of the gradual variation of molecular orientation and lack of space due to severe confinement. This competition prevents the number of strata from increasing by one as s_z becomes larger and causes the fictitious disappearance of already existing strata discussed in the preceding section in conjunction with Figs. 3(c)–3(e). The parallel results in Fig. 5(c)–5(e), however, clearly demonstrate that there is no such disappearance but that the orientation changes so that the middle stratum, which still exists, becomes rather diffuse and is buried in the plot of $\overline{\rho(z;s_z)}$ in Fig. 3(d).

D. The normal stress

Clearly, the previously discussed structural features of confined liquid-crystal films must manifest themselves in materials properties, too. To this end, perhaps the most interesting quantity is the normal component of the stress tensor T_{zz} which can be measured in principle in SFA experiments [4,5]. It is obtained here from both virial and force expressions [see Eqs. (30), (37)]. Results are plotted in Fig. 6 as a function of wall separation s_z. Generally speaking, T_{zz} as well as its components T_{zz}^{FF} and T_{zz}^{FW} from the virial expression are damped oscillatory functions of s_z. As before in the classification of significant structural changes, the quantity r proves useful to distinguish different regimes in the curve $T_{zz}(s_z)$ which in turn demonstrates the close relation between T_{zz} and the microscopic structure of the film. We therefore identify different zones in Fig. 6 according to the classification scheme introduced in Fig. 2. It turns out that in regions where $r<1$, T_{zz} increases with s_z while it decreases whenever $r>1$. This makes sense intuitively because T_{zz} may be viewed as a measure of ''ease'' with which the film can imbibe additional matter from a reservoir as s_z increases. It is then plausible that the ''rate'' of imbibition in the confined film relative to the bulk (namely, r) should be less than one until T_{zz} has reached a maximum. If, on the other hand, a structural change permits the film to imbibe matter more easily beyond a certain threshold (i.e., if T_{zz} decays beyond a maximum value) r should exceed one until T_{zz} assumes a new minimum. The plot in Fig. 6 confirms this notion.

Figure 6 also shows that T_{zz} has less distinct extrema compared with earlier results for a ''simple'' fluid confined between structured walls (see Fig. 3.4.a in [7]). Viewing

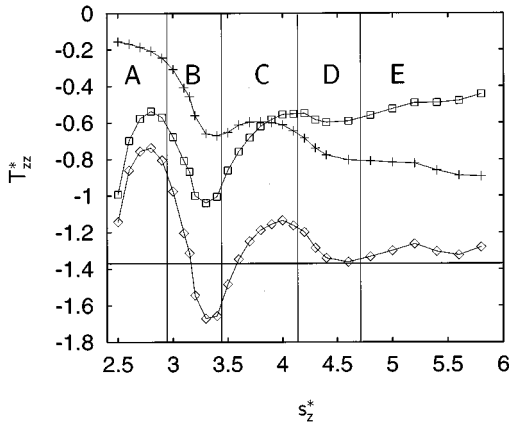

FIG. 6. The normal stress component T_{zz} as a function of distance s_z between the walls from Eq. (30) ($\diamond$), T_{zz}^{FW} ($\square$), T_{zz}^{FF} ($+$). Lines are intended to guide the eye. The horizontal line represents the negative pressure $-P_b$ of a bulk fluid at the same T and μ. See Fig. 2 for a definition of zones A–E.

T_{zz} as a measure of stratification, one can rationalize this observation in terms of the more pronounced geometric mismatch between the crystallographic structure of the walls and the molecular structure of Gay-Berne molecules in comparison with previous models in which films of spherically symmetric molecules were confined between fcc (100) walls. In addition to the geometric mismatch, stratification is reduced here further by molecular orientability according to the discussion in the preceding section. The influence of such geometric factors has also been noted experimentally by Gee *et al.* [5], who observed in SFA experiments with certain branched hydrocarbon films confined between mica surfaces that oscillations are completely absent in a plot of the analog of T_{zz} versus s_z while many very distinct oscillations are detected if the film is composed of long-chain hydrocarbons which can adjust themselves more easily to the rather rigid and symmetric mica structure because of their greater flexibility.

One may also verify from Fig. 6 that the sum $T_{zz}^{FF}+T_{zz}^{FW}$ agrees nicely with the force expression for T_{zz} as required (see Sec. III A). The agreement is nearly perfect up to $s_z^*\simeq 4.2$ and does not exceed 4% even at the largest wall separation. However, we deliberately refrain from plotting T_{zz} from Eq. (37) along with its force counterpart because we do not want to overload Fig. 6 and, more importantly, because plotting the components T_{zz}^{FF} and T_{zz}^{FW} separately permits more interesting conclusions. First, one notices from Fig. 6 that even at $s_z^*=5.8$, T_{zz} has not reached its large-system limit $-P_b$ [see Eq. (52)] and, furthermore, does not exhibit a clear tendency toward it. This can be understood from the plot of T_{zz}^{FF} and T_{zz}^{FW} in Fig. 6 which are almost monotonous functions of s_z beyond $s_z^*\simeq 4.6$ having small, nearly equal slopes of opposite sign. Thus when summed these slopes cancel partially resulting in an even weaker global dependence of T_{zz} on s_z which we are unable to detect given the accuracy of the data. Second, it follows from Eq. (52) that the limiting value $-P_b$ should be assumed by T_{zz}^{FF} alone, that is, $\lim_{s_z\to\infty}T_{zz}^{FW}=0$. The plots in Fig. 6 clearly show that $s_z^*=5.8$ is apparently way below the large-system limit because $|T_{zz}^{FW}(s_z^*=5.8)/P_b|\simeq 0.32$ is still quite substantial. This raises the interesting question: how large is the limiting value $s_z^{\lim}$ at which Eq. (52) *approximately* holds [i.e., at which $T_{zz}^{FW}(s_z^{\lim})\simeq 0$]? The question may be answered if one realizes from Eq. (36) that beyond a certain film thickness (i.e., s_z) W_{zz}^{FW} reaches a constant value due to the finite range of the film-wall interaction potential. For thicker films it then seems reasonable to expect [see Eq. (37c)] T_{zz}^{FW} to increase according to

$$T_{zz}^{FW}=-\frac{a}{s_z}, \tag{60}$$

where a is some constant. From simulation data at various values of s_z we estimate this constant in Table II which turns out not to vary appreciably over the range of wall separations considered so that Eq. (60) apparently holds. Based on the estimate of a one can calculate a limiting value $s_z^{\lim}$ at which Eq. (52) is approximately satisfied. Taking $|T_{zz}^{FW}/P_b|\leqslant 0.01$ as a reasonable but arbitrary criterion, $(s_z^{\lim})^*\simeq 190$ is obtained, which is much larger than the range of film-wall interactions indicating the importance of cooperative phenomena for materials properties of confined films. This is substantiated further by the slow decay of T_{zz}^{FF} which at $s_z^*=12$ has reached only 83% of its limiting value $-P_b$ [see Eq. (52)]. That it is not unreasonable to expect an impact of the walls over distances of several tens of molecular ''diameters'' is corroborated also by results for self-diffusion in a ''simple'' fluid confined between fcc (100) walls. At $s_z^*=30$ the self-diffusion coefficient $D_\parallel$ for the diffusion of film molecules located halfway in between the walls and moving in a ''plane'' parallel with the walls exceeds its bulk counterpart significantly (see Fig. 5.3 in [7]).

TABLE II. GCEMC results for the film-wall contribution to the normal stress T_{zz}^{FW} for various distances s_z between the walls. Parameter a and $s_z^{\lim}$ are calculated from Eq. (60) according to the criterion $|T_{zz}^{FW}/P_b|\leqslant 0.01$.

s_z	T_{zz}^{FW}	a	$s_z^{\lim}$
4.8	−0.559	2.68	196
5.8	−0.443	2.57	188
8.0	−0.323	2.58	188
12.0	−0.216	2.60	190

V. CONCLUDING REMARKS

In this paper we present results from GCEMC simulations of molecularly thin confined Gay-Berne films. These are simulations of a confined liquid crystal under conditions encountered in complementary XSFA experiments [12]. In these experiments the confined film is open to a bulk reservoir with which it exchanges matter, work, and heat. To mimic these conditions in a computer simulation, the grand canonical ensemble is well suited because it permits one to compute properties of both film and bulk reservoir separately under experimentally relevant conditions, i.e., fixed temperature T and chemical potential μ in both subsystems. This approach views the film as infinitely large in the plane par-

allel to the walls and therefore ignores edge effects at film-bulk contact, which we believe to be a rather mild assumption.

The results presented here give clear evidence of a high degree of structural complexity in liquid-crystal films on account of the orientability of film molecules. Orientations can be analyzed best in terms of density-alignment histograms $h(z,u_z^2;s_z)$ since Gay-Berne molecules are nonpolar. The histograms show that the microscopic structure of molecularly thin liquid-crystal films is a consequence of a competition between the orientation favored by the film-wall interaction potential and spatial constraints, that is, lack of space. The observed orientations are solely due to the presence of (discrete) walls because the thermodynamic state of a corresponding Gay-Berne bulk phase pertains to the isotropic phase where no particular orientation is distinguished. However, details of wall-induced orientations in a liquid-crystal film will depend on the orientation favored by the film-wall potential, that is, the choice of ϵ_{fw}^s and κ_{fw}' in Eq. (11). Depending on their value, homeotropic or parallel orientations of the microscopic director $\hat{\boldsymbol{u}}$ with respect to the plane of the walls may be realized which then have to compete with packing effects. In this paper we concentrate on walls which tend to align film molecules in parallel planes. In a separate publication we plan to study the impact of other parameter sets for the film-wall potential on the microscopic structure of confined liquid-crystal films [34]. Within the context of the present study, however, it seems worthwhile to stress that unlike $h(z,u_z^2;s_z)$ the (reduced) local density $\overline{\rho}(z;s_z)$ is not too well suited to characterize the microscopic structure of a confined liquid-crystal film under current conditions. This is because $\overline{\rho}(z;s_z)$ is primarily a measure of stratification which is not too strong here in most cases. Compared with films composed of ''simple'' molecules (see Fig. 3.5 in [7]) individual strata appear generally to be spatially less well localized and overlap [cf. Figs. 3(b)–3(f)]. The reduced degree of stratification is also seen in T_{zz} which exhibits less distinct oscillations with varying s_z compared with a film of ''simple'' fluids. However, $T_{zz}(s_z)$ compares *qualitatively* well with results obtained in SFA experiments which involve a liquid-crystal film whose corresponding bulk phase is isotropic, too [40].

Besides confinement and mismatch between wall and film structure, the thermodynamic state has a significant impact on stratification. For example, if the thermodynamic state pertains to a smectic or nematic bulk phase, more stratified films are conceivable. Smectic films, which are the subject of prime interest in recent XSFA experiments [6,11,12], are, however, difficult (if not impossible) to investigate within the present GCEMC framework because of their large density and high degree of order, which renders the conventional addition-removal step of the GCEMC algorithm very inefficient.

ACKNOWLEDGMENTS

We are indebted to Professor Siegfried Hess (Technische Universität Berlin) for his generosity, constant interest, and support of this work. Professor M.P. Allen (University of Bristol), Professor D.J. Diestler (University of Nebraska-Lincoln), and Professor S. Hess are acknowledged for critically reading the manuscript and for discussions which we enjoyed during the course of this work. We are grateful to the Sonderforschungsbereich 331 ''Anisotrope Fluide'' and the Deutsche Forschungsgemeinschaft (DFG) for financial support. Computations were carried out on the Cray J932 of the Konrad-Zuse-Rechenzentrum (Berlin) which we acknowledge for a generous allotment of computer time.

[1] *Liquid Crystals, Applications and Uses*, edited by B. Bahadur (World Scientific, Singapore, 1990), Vol. 1.
[2] *Materials Research Society Bulletin*, edited by J. F. Belak (Materials Research Society, Pittsburgh, 1993), Vol. 18.
[3] R. Eidenschink, Angew. Chem. **100**, 1639 (1988).
[4] J. N. Israelachvili, *Intermolecular and Surface Forces* (Academic Press, London, 1992).
[5] M. L. Gee, P. M. McGuiggan, J. N. Israelachvili, and A. M. Homola, J. Chem. Phys. **93**, 1895 (1990).
[6] I. Koltover, S. H. J. Idziak, C. R. Safinya, S. Steinberg, J. N. Israelachvili, and K. S. Liang, in *Dynamics in Small Confining Systems*, edited by J. M. Drake *et al.*, MRS Symposia Proceedings No. 366 (Materials Research Society, Pittsburgh, 1995), p. 101.
[7] M. Schoen, *Computer Simulation of Condensed Phases in Complex Geometries* (Springer-Verlag, Heidelberg, 1993).
[8] M. Schoen, Ber. Bunsenges. Phys. Chem. **100**, 1355 (1996).
[9] M. Schoen, D. J. Diestler, and J. H. Cushman, J. Chem. Phys. **101**, 6865 (1994).
[10] M. Schoen, J. Chem. Phys. **105**, 2910 (1996).
[11] S. H. J. Idziak, C. R. Safinya, R. S. Hill, M. Ruth, H. E. Warriner, K. E. Kraiser, K. S. Liang, and J. N. Israelachvili, Science **264**, 1915 (1994).
[12] S. H. J. Idziak, I. Koltover, J. N. Israelachvili, and C. R. Safinya, Phys. Rev. Lett. **76**, 1477 (1996).
[13] A. Kilian and S. Hess, Liq. Cryst. **8**, 465 (1990).
[14] T. Gruhn and S. Hess, Z. Naturforsch. Teil A **51**, 1 (1996).
[15] M. D. Dadmun and M. Muthukumar, J. Chem. Phys. **101**, 10038 (1994).
[16] M. P. Allen and D. Frenkel, Phys. Rev. A **37**, 1813 (1988); **42**, 3641 (1990).
[17] A. P. J. Emerson and C. Zannoni, J. Chem. Soc. Faraday Trans. **91**, 3441 (1995).
[18] D. Frenkel and R. Eppenga, Phys. Rev. A **31**, 1776 (1985).
[19] J. G. Gay and B. J. Berne, J. Chem. Phys. **74**, 3316 (1981).
[20] E. de Miguel, L. F. Rull, M. K. Chalam, and K. E. Gubbins, Mol. Phys. **71**, 1223 (1990).
[21] J. Stelzer, L. Longa, and H. R. Trebin, J. Chem. Phys. **103**, 3098 (1995).
[22] M. K. Chalam, K. E. Gubbins, E. de Miguel, and L. F. Rull, Mol. Sim. **7**, 357 (1991).
[23] J. Stelzer, L. Longa, and H. R. Trebin, in *Proceedings of 24. Freiburger Arbeitstagung Flüssigkristalle*, edited by G. Baur (Albert-Ludwigs-Universität, Freiburg, 1995).
[24] D. J. Diestler, M. Schoen, and J. H. Cushman, Science **262**, 545 (1993).

[25] B. J. Berne and P. Pechukas, J. Chem. Phys. **56**, 4213 (1972).
[26] M. P. Allen and D. J. Tildesley, *Computer Simulation of Liquids* (Oxford University Press, Oxford, 1989).
[27] D. J. Diestler, M. Schoen, J. E. Curry, and J. H. Cushman, J. Chem. Phys. **100**, 9140 (1994).
[28] D. A. McQuarrie, *Statistical Mechanics* (Harper & Row, New York, 1976).
[29] C. G. Gray and K. E. Gubbins, *Theory of Molecular Fluids, Vol. 1: Fundamentals* (Clarendon Press, Oxford, 1984).
[30] G. Arfken, *Mathematical Methods for Physicists*, 3rd ed. (Academic Press, London, 1985), p. 478.
[31] M. Schoen, S. Hess, and D. J. Diestler, Phys. Rev. E **52**, 2587 (1995).
[32] D. J. Diestler and M. Schoen, J. Chem. Phys. **104**, 6784 (1996).
[33] S. A. Rice and P. Gray, *The Statistical Mechanics of Simple Liquids* (Interscience Publishers, New York, 1965), Chap. 4.
[34] T. Gruhn and M. Schoen (unpublished).
[35] J. P. Hansen and I. R. McDonald, *Theory of Simple Liquids*, 2nd ed. (Academic Press, London, 1986), p. 30.
[36] T. L. Hill, *Statistical Mechanics, Principles and Selected Applications* (Dover, Mineola, 1987), Chap. 4.20.
[37] H. B. Callen, *Thermodynamics* (John Wiley & Sons, New York, 1960), Chap. 7.
[38] V. Y. Antonchenko, V. V. Ilyin, N. N. Makovsky, A. N. Pavlov, and V. P. Sokhan, Mol. Phys. **52**, 345 (1984).
[39] I. K. Snook and W. van Megen, J. Chem. Phys. **72**, 2907 (1979).
[40] L. Moreau, P. Richetti, and P. Barois, Phys. Rev. Lett. **73**, 3556 (1994).